Characterization of a shaped isolated attosecond pulse and retrieval of infrared-laser-related information using high-order-harmonic-generation streaking spectra

Kan Wang [1], Yong Fu[1], Baochang Li[1], Xiangyu Tang[1], Zhong Guan[1], Bincheng Wang[1], C. D. Lin [2], and Cheng Jin [1,3,*]

[1]*Department of Applied Physics, Nanjing University of Science and Technology, Nanjing, Jiangsu 210094, China*

[2]*J. R. Macdonald Laboratory, Department of Physics, Kansas State University, Manhattan, Kansas 66506, USA*

[3]*MIIT Key Laboratory of Semiconductor Microstructure and Quantum Sensing, Nanjing University of Science and Technology, Nanjing, Jiangsu 210094, China*

(Received 14 September 2023; accepted 29 January 2024; published 20 February 2024)

An all-optical method for directly reconstructing the spectral phase of an isolated attosecond pulse (IAP) has been proposed recently [New J. Phys. **25**, 083003 (2023)]. This method is based on high-harmonic-generation (HHG) streaking spectra generated by an IAP and a time-delayed intense infrared (IR) laser, which can be accurately simulated by an extended quantitative rescattering model. Here, we extend the retrieval algorithm in this method to successfully retrieve the spectral phase of a shaped IAP, which has a spectral minimum, a phase jump about π, and a "split" temporal profile. We then reconstruct the carrier-envelope phase of the IR laser from HHG streaking spectra. Finally, we discuss retrieval of the phase of high harmonics by the intense IR laser alone using the Fourier transform of HHG streaking spectra.

DOI: 10.1103/PhysRevA.109.023117

I. INTRODUCTION

Revolution of attosecond science has enabled to investigate and manipulate ultrafast electronic dynamics in atoms, molecules, and solids with an unprecedented temporal resolution [1–4]. As its foundation, the technique of high-order harmonic generation (HHG) from a gas medium has become mature and stable to efficiently produce attosecond pulse trains [5] or isolated attosecond pulses (IAPs) [6]. Especially, with development of mid-infrared laser and phase-locking technologies, IAPs with ultrashort temporal duration down to a few tens of attoseconds can be obtained up to the water-window spectral region [7,8]. To fully characterize an IAP, the so-called attosecond streaking method is commonly used, in which the IAP first ionizes an atomic target and then a moderate infrared (IR) laser is applied to modulate photoelectron spectra [9]. A number of algorithms have been developed to retrieve the IAP and the IR laser from time-delay dependent photoelectron spectra, including FROG-CRAB (frequency-resolved optical gating for complete reconstruction of attosecond bursts) [10], PROOF (phase retrieval by omega oscillation filtering) [11], and PROBP (phase retrieval of broadband pulses) [12,13].

Alternatively, the IAP can be combined with a time-delayed, few-cycle intense IR laser to perturb or reform the HHG process. Modulated harmonic spectra with the time delay between the IAP and the IR laser are called HHG streaking spectra, which provide with an all-optical scheme to retrieve the IAP [14]. The IAP in the extreme ultraviolet (XUV) can actually affect well-known three steps in the HHG process differently. For instance, the XUV pulse with the high photon energy can populate inner-shell electrons to excited states through single-photon ionization, leading to an increase in the ionization energy, which in turn affects efficiency and the cutoff energy of harmonic emission [15]. The IAP can act in the propagation step and cause multiple scatterings of active electrons, thereby influencing low-energy high harmonics [16]. If electrons absorb high-energy XUV photons in the returning step, the HHG plateau region could be broadened [17]. Furthermore, XUV pulses can be employed to selectively control the specific electron trajectory for modulating the harmonic field [18]. XUV parametric amplification (XPA) has also been achieved when the XUV pulse is combined with the intense IR laser, attributing to the nonadiabtic forward scattering of the electron wave packet [19]. To precisely simulate HHG streaking spectra under interplay of the IAP and the time-delayed IR laser, we have developed an extended quantitative rescattering (EQRS) model [14] by greatly improving the strong-field approximation (SFA) [16,20,21]. Based on the EQRS model and the SFA, we derived a retrieval algorithm for successfully reconstructing IAPs in both the XUV and soft X-ray regions from HHG streaking spectra [22]. However, there are still some challenging questions not yet resolved. Can one retrieve information of the IR laser from HHG streaking spectra, for example, the carrier-envelope phase (CEP) of the IR laser? It is known that reconstruction of the IR laser is feasible in the traditional method of attosecond streaking camera [12]. Can one obtain information of HHG by the intense IR laser alone?

It has been established that the minimum structure existing in atomic HHG spectra can be directly related to that in the photorecombination cross section (PRCS) [23]. A typical example is the Cooper minimum (CM) in the HHG spectra of Ar [24–27]. By spectral filtering high harmonics around the CM, the temporal XUV pulse would be severely shaped [28]. The CM in the HHG spectrum has also been observed in various

*Corresponding author: cjin@njust.edu.cn

atoms [29] and molecules [30–32]. Recently, Jin *et al.* [33,34] reported on control of the minimum in the HHG spectra of aligned CO_2 molecules by adjusting the degree of alignment. Such minimum is similar to the CM, called the "structural minimum," and can be explained by the alignment averaged PRCS. Since the amplitude of the averaged PRCS varies rapidly and its phase changes near π around the minimum, the resulting temporal attosecond pulses are greatly shaped and can be tuned. Can such structured attosecond pulses also be reconstructed from HHG streaking spectra?

To answer the above questions, in this paper, we will extend and improve the all-optical retrieval algorithm based on HHG streaking spectra. We will specifically focus on how to correctly retrieve the spectral phase of a shaped isolated attosecond pulse in Sec. II, how to identify the CEP of the IR laser from HHG streaking spectra in Sec. III, and how to obtain the phase of high harmonics by the IR laser alone in Sec. IV. Finally, conclusions will be given in Sec. V.

II. RECONSTRUCTION OF THE SPECTRAL PHASE OF SHAPED ATTOSECOND PULSES

First, we simulate HHG streaking spectra of the Ne atom under a shaped IAP and a time-delayed IR laser. Note that we choose the neon atom as the target one because it has a smooth structure in the PRCS, see Fig. 2(d) in Ref. [35]. The PRCS is a key ingredient in the HHG process according to the quantitative rescattering (QRS) model. Thus, any peculiar features in the HHG streaking spectra can be traced back to the unknown XUV pulse. In addition, the neon atom has a bigger PRCS compared to the commonly used He atom, resulting in stronger HHG streaking spectra. The shaped IAP exhibits an extreme minimum centered at 60 eV in the spectral amplitude and a significant phase jump as shown in Fig. 1(a). These data are taken from Ref. [33] when HHG of aligned CO_2 molecules is generated under the alignment degree of 0.40 and the pump-probe angle of 0°. In the simulations, we use an IR laser with the wavelength of 800 nm, the full-width-at-half-maximum (FWHM) duration of 5 fs, the peak intensity of 2.5×10^{14} W/cm^2, and the CEP of 0. We set the peak intensity of the shaped IAP as 2.5×10^{11} W/cm^2, and calculate HHG streaking spectra with the time delay between the IAP and IR laser by using the EQRS model. Results are shown in Fig. 1(b). The modulation structure can be clearly observed with the time delay if spectral amplitudes of the shaped IAP are stronger, for example, around 50 eV and 67 eV, but it is difficult to distinguish at the minimum energy, i.e., at 60 eV.

We then apply the all-optical phase reconstruction method developed in Ref. [22]. Note that we focus on retrieval of the spectral phase of the shaped IAP only while the spectral intensity can be easily measured by the spectrometer, which is assumed known. At each photon energy, by fitting the time-delay modulated spectrum, we obtain the time delay corresponding to the maximum modulation. In Ref. [22], we have derived that the peak of the HHG modulated spectrum is coincident with that of the IR intensity profile of $E_{\rm IR}^2(\alpha - \tau)$, where α is the derivative of the XUV spectral phase with the time. For two selected photon energies, we show comparisons of the HHG modulated spectrum and the envelope of $E_{\rm IR}^2(\alpha - \tau)$ as a function of the time delay τ in Figs. 1(c) and 1(d). At 55.6 eV, which is far away from the spectral minimum of the shaped IAP, the peak position of the HHG modulated spectrum reaches an excellent agreement with that of the IR intensity envelope, see Fig. 1(c). However, at 60.1 eV, which is at the spectral minimum, the HHG modulated spectrum shows a completely different period of modulation, and its peak position is quite away from that of the IR intensity envelope, see Fig. 1(d). Thus, around the spectral minimum of the shaped IAP, retrieved time delays corresponding to the maximum modulation of the HHG modulated spectrum are not correct. We then use the retrieved time delays to construct the curve of the group delay, as shown by the red dashed line in Fig. 1(e), which deviates much from the input one (black solid line) around the minimum. This leads to some big errors in the reconstructed phase of the shaped IAP (purple dot-dashed line) compared to the input one (blue dotted line). We show the retrieved XUV pulse in time (red dashed line) in Fig. 1(f), and the input pulse (black solid line) is also plotted for comparison. The retrieval procedure returns errors in peak positions, relative peak intensities, and widths of the temporal shaped pulse. Such errors cannot be acceptable for characterizing the shaped IAP. Note that errors in the group delay cannot be fixed by simply increasing the number of discrete points in the energy and time delay.

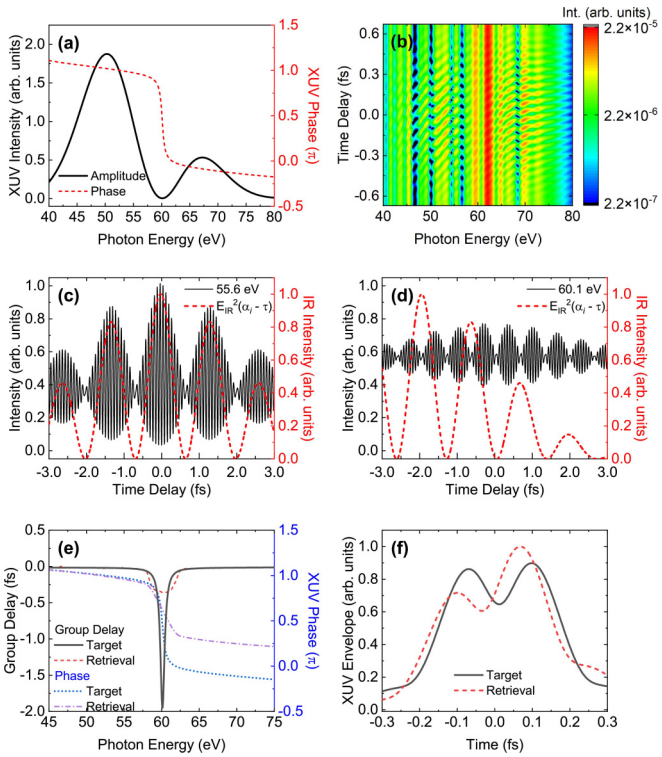

FIG. 1. (a) The spectral amplitude and phase of a shaped attosecond pulse. (b) HHG streaking spectra calculated by the EQRS model. The color bar represents the spectral intensity (Int.). (c, d) HHG modulated spectra (black solid lines) and intensity profiles of $E_{\rm IR}^2(\alpha - \tau)$ (red dashed lines) at two selected photon energies. (e) The group delay and spectral phase obtained by the original phase reconstruction method in comparison with input values. (f) Comparison of the reconstructed temporal profile of the shaped IAP with the input one.

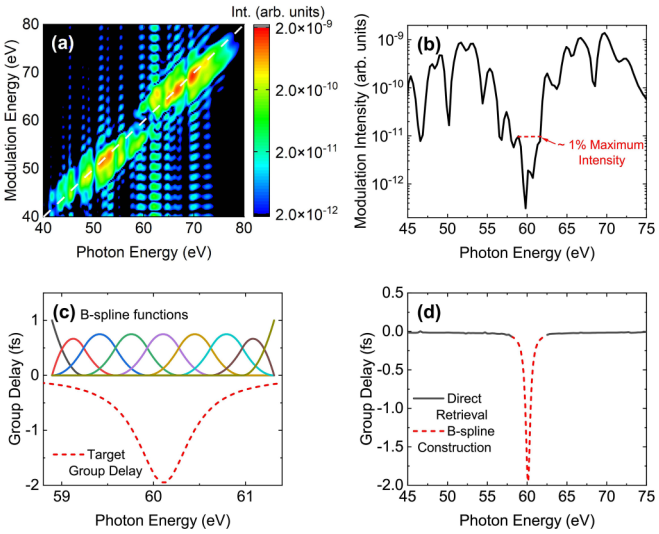

FIG. 2. (a) Modulated energy spectra obtained by performing the Fourier transformation with respect to the time delay. The color bar represents the spectral intensity (Int.). (b) The intensity of the modulated spectrum with the photon energy along the diagonal line. (c) B-spline basis functions and the target group delay of the shaped IAP. (d) The target group delay contains two parts: one is retrieved directly using the original phase reconstruction method (black solid line) and the other is reconstructed using the newly developed B-spline function expansion method (red dashed line) as shown in (c).

To explain errors occurring in extraction of the group delay, we make a transformation of HHG streaking spectra in Fig. 1(b). For each photon energy ω, the Fourier transform with respect to the time delay is performed, which can be expressed as

$$S'(\omega, \omega_{\mathrm{mod}}) = \frac{1}{2\pi}\int_{\tau_1}^{\tau_2} S(\omega, \tau) e^{i\omega_{\mathrm{mod}}\tau} d\tau, \tag{1}$$

where $S(\omega, \tau)$ represents the HHG streaking spectrum and $S'(\omega, \omega_{\mathrm{mod}})$ is the modulated energy spectrum after the Fourier transform. ω_{mod} is the modulation frequency, reflecting the frequency component of the modulation structure, and τ_1 and τ_2 are the start and end time delays for the integral, respectively. Modulated energy spectra are shown in Fig. 2(a). To ensure the accuracy of modulated energy spectra, we choose the width of the integration window as a half IR optical cycle, which is one full modulation period. And integration covers the strongest modulated HHG spectra and is centered at the maximum modulation. One can see that considerable modulation intensities are primarily distributed along a diagonal line for most photon energies. This indicates that the major modulation frequency in the HHG streaking spectra is about the same as the spectral frequency of the IAP. However, for photon energies around 60 eV, the peak of the modulation intensity splits into two components along the modulation energy, due to the phase jump of the XUV pulse, not the lack of the XUV signal. This also means that the time delay in the HHG streaking spectra cannot be directly related to the spectral energy around the minimum of the XUV pulse, thus the previous phase reconstruction method is not applicable.

We next improve the phase reconstruction method, specifically, eliminating errors in the reconstructed group delay. From Fig. 1(c), one can see that reconstructed results only need to be fixed in a narrow energy region around the spectral minimum of the IAP. We first determine the range of such a photon-energy region. In Fig. 2(b), the modulation intensity along the diagonal line in Fig. 2(a) is plotted as a function of the photon energy. By testing various shaped IAPs, a photon-energy region is selected where modulation intensities are within 1% of the maximum value (red dashed line) as shown in Fig. 2(b). We then determine how to construct the group delay in this energy region, which has a sharp structure. We adopt the B-spline function as a basis to expand the group delay in the following:

$$f_{gd}(\omega) = \sum_{i=1}^{n} g_i B_i^k(\omega), \tag{2}$$

where g_i is the expansion factor for the i-th B-spline function with the k-th order. It is defined as

$$B_i^k(\omega) = \begin{cases} 1, & \omega_i \leqslant \omega \leqslant \omega_{i+1} \\ 0, & \text{otherwise,} \end{cases} \tag{3}$$

$$B_i^k(\omega) = \frac{\omega - \omega_i}{\omega_{i+k-1} - \omega_i} B_i^{k-1}(\omega) + \frac{\omega_{i+k} - \omega}{\omega_{i+k} - \omega_{i+1}} B_{i+1}^{k-1}(\omega). \tag{4}$$

Here, ω_i are frequency knot points. Details of B-spline functions can be founded in Refs. [12,36]. Figure 2(c) illustrates B-spline basis functions and the target group delay. Here, we utilize nine B-spline functions with the ninth order. Thus, nine coefficients g_i in Eq. (2) need to be determined. The resulted group delay in the narrow energy region can be combined with that obtained by the previous phase construction method as schematically illustrated in Fig. 2(d). We also need to determine another parameter β, connecting the phase over the entire spectral region. Then, we employ a genetic algorithm (GA) to optimize coefficients g_i and the parameter β. In each iteration, by combing the spectral amplitude and the phase given by $\{g_i, \beta\}$, we obtain the shaped IAP in time, calculate HHG streaking spectra by using the EQRS model, and simulate modulated energy spectra according to Eq. (1). The population size is chosen to be 5 and the maximum number of generation is set to be 1000–2000 to guarantee convergence. Finally, we give the error (or fitness) function in the optimization. We choose the phase of modulated spectra $\phi_{\mathrm{mod}}(\omega)$ as a function of the photon energy along the diagonal line in Fig. 2(a). This phase is plotted in Fig. 3(d). The error function can be expressed as

$$F_{\mathrm{error}}(g_i, \beta) = \frac{1}{m}\sum_{m} |\phi_{\mathrm{mod},0}(\omega_m) - \phi_{\mathrm{mod},1}(\omega_m)|, \tag{5}$$

where $\phi_{\mathrm{mod},0}(\omega_m)$ and $\phi_{\mathrm{mod},1}(\omega_m)$ represent the phase of the input and reconstructed modulated energy spectrum, respectively. Photon energy sampling points ω_m in the whole spectral region are chosen as $m = 100$.

For the shaped IAP displayed in Fig. 1, we follow the above steps and obtain reconstructed results in Fig. 3. Comparison of the input and reconstructed group delay and spectral phase of the IAP is present in Figs. 3(a) and 3(b), respectively. Corre-

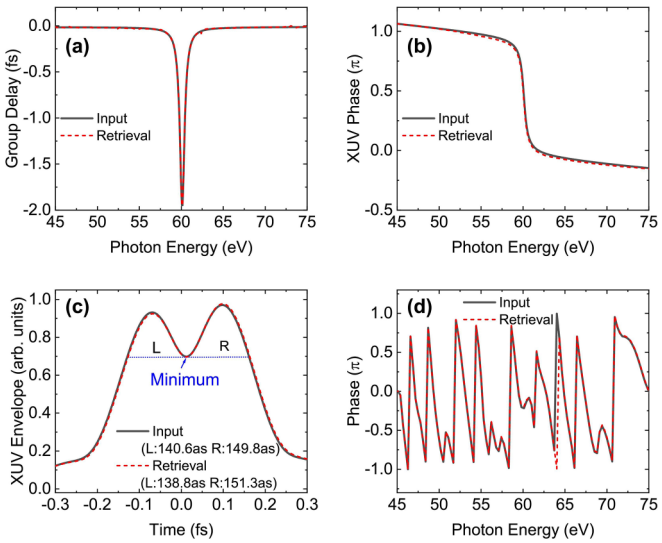

FIG. 3. Comparison of retrieved results with input ones: (a) the group delay, (b) the spectral phase, and (c) the temporal profile of the shaped IAP, and (d) the phase of modulated energy spectra.

sponding temporal profiles are shown in Fig. 3(c). We use a different way to define the width of the double peaked pulse. We identify the position of the minimum in the temporal profile, use its intensity as a reference, and define widths of left and right peaks separately. Compared to the input information (i.e., the width of the left peak is 140.6 as and that of the right one is 149.8 as), reconstructed widths are 138.8 as and 151.3 as for the left and right peak, respectively, which have an error of less than 2%. We also compare the input and reconstructed phase of modulated spectra in Fig. 3(d). Dramatic change in the spectral phase around the minimum can be reflected in the phase of modulated spectra. Choosing the phase in the fitness function greatly improves the accuracy of the retrieval procedure.

We then choose another two shaped IAPs with different temporal shapes and spectral phase around the minimum and test the validity of our improved reconstruction method. As demonstrated by Jin *et al.* [33], such shaped pulses can be obtained by tuning the alignment degree of CO_2 molecules or by adjusting the pump-probe angle. Simulated HHG streaking spectra by using the EQRS model are shown in Figs. 4(a) and 4(b), with corresponding spectral amplitude distributions being plotted on the top. We apply the Fourier transform with respect to the time delay and obtain modulated energy spectra in Figs. 4(c) and 4(d). These spectra exhibit typical interference patterns and the splitting around spectral minima. Results of the group delay and the spectral phase returned by the improved reconstruction method are shown in Figs. 4(e) and 4(f), respectively. There are some deviations in the reconstructed results of the group delay, especially in Fig. 4(f). This is because the photon energy range for executing the expansion of B-spline functions is different, but the used number of B-spline functions is fixed. Such deviations do not affect the accuracy of the reconstructed phase and temporal pulse duration. Temporal profiles of two reconstructed pulses are plotted in Figs. 4(g) and 4(h). For the fist IAP, the retrieved width of the left peak is 139.7 as compared to the input value of 134.8 as, and it is 52.8 as for the right peak while the input width is 60.8 as. The error in the retrieved width is increased for the right peak because its peak intensity is in close proximity to the minimum one. For the second IAP, the reconstructed width of the left peak is 206.8 as (compared to the input value of 208.1 as) and the right one is 135.3 as (compared to the input value of 136.5 as), with the error less than 1%.

III. RECONSTRUCTION OF THE CEP OF AN IR LASER FROM HHG STREAKING SPECTRA

We then discuss whether the CEP of a few-cycle intense IR laser is imprinted in the HHG streaking spectra. In Ref. [22],

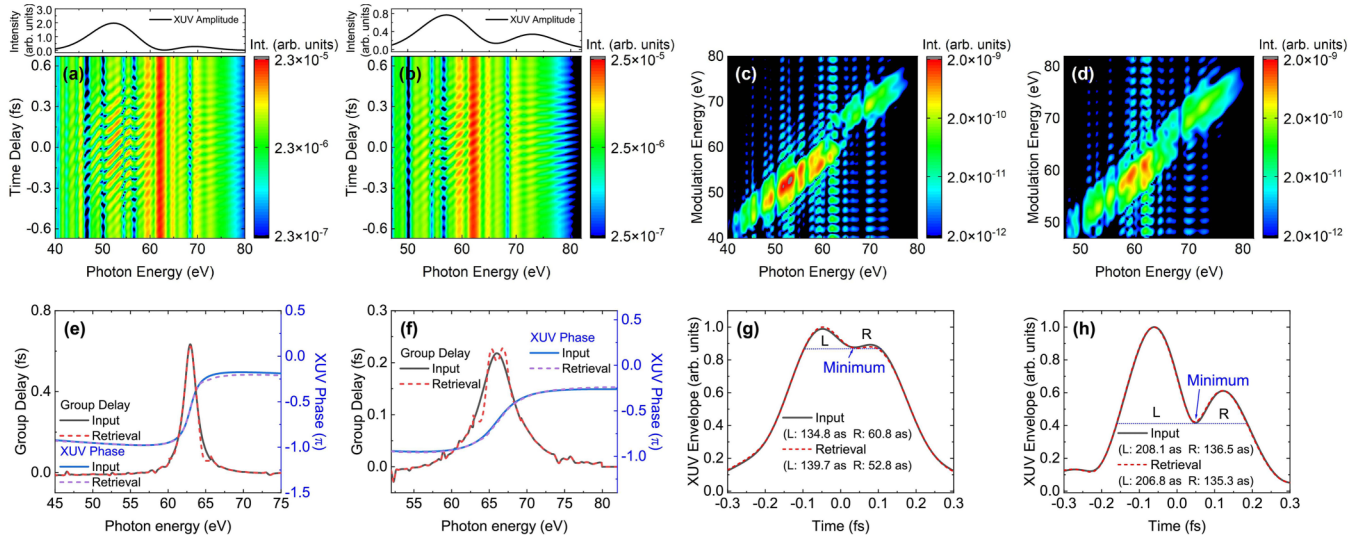

FIG. 4. (a, b) HHG streaking spectra and (c, d) modulated energy spectra through the Fourier transform with respect to the time delay by using two shaped IAPs, respectively. Spectral amplitudes of two IAPs are plotted on the top in (a) and (b). Comparison of retrieved results of two shaped IAPs with input ones: (e, f) the group delay and spectral phase, and (g, h) the temporal profile.

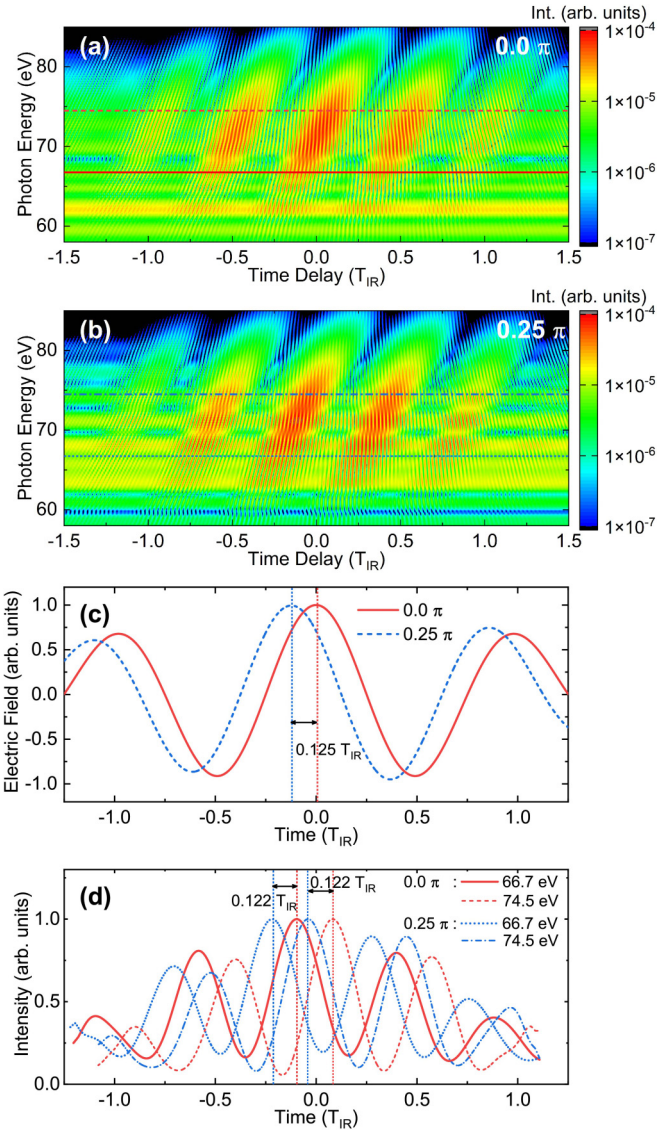

FIG. 5. HHG streaking spectra generated by the IR laser with different CEPs: (a) 0.0 π and (b) 0.25 π. Corresponding electric fields of the IR laser are shown in (c). (d) Envelopes of the time-delayed HHG modulation intensity for different combinations of the CEP and the photon energy: 0.0 π, 66.7 eV (red solid line); 0.0 π, 74.5 eV (red dashed line); 0.25 π, 66.7 eV (blue dotted line); and 0.25 π, 74.5 eV (blue dot-dashed line). $T_{\rm IR}$ is the optical cycle of the IR laser.

we derived that the coupling term of the IAP and the IR laser in the induced dipole moment can be written as

$$|x_2(\omega,\tau)|^2 \propto E_{\rm IR}^2(\alpha-\tau), \tag{6}$$

where α is the derivative of the XUV spectral phase with the time. In this equation, the CEP $\Phi_{\rm CEP}$ of the IR laser is assumed as 0. When it becomes arbitrary, Eq. (6) can be extended as

$$|x_2(\omega,\tau)|^2 \propto E_{\rm IR}^2(\alpha-\tau+\Phi_{\rm CEP}/\omega_{\rm IR}), \tag{7}$$

where $\omega_{\rm IR}$ is the angular frequency of the IR laser. Thus, the time delay corresponding to the maximum modulation can be

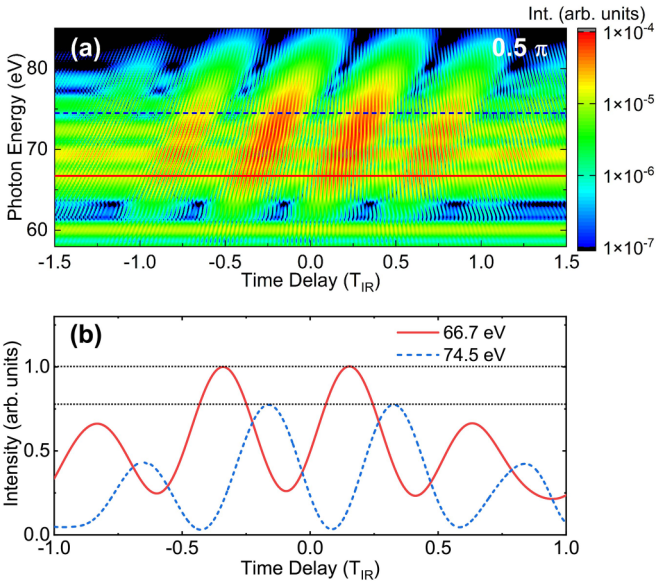

FIG. 6. (a) HHG streaking spectra when the CEP of the IR laser is 0.5 π. (b) Envelopes of the time-delayed HHG modulation intensity at different photon energies: 66.7 eV (red solid line) and 74.5 eV (blue dashed line).

written as

$$\tau(\omega) = \alpha + \frac{\Phi_{\rm CEP}}{\omega_{\rm IR}}. \tag{8}$$

Equation (8) means that the time delay corresponding to the maximum modulation intensity in the HHG streaking spectra is varied with the CEP of the IR laser.

To test it, we choose a regular chirped IAP centered at 71.3 eV with a spectral bandwidth of 9 eV, and set the CEP of the IR laser as 0 and 0.25 π, respectively. The resulting HHG streaking spectra by using the EQRS model are shown in Figs. 5(a) and 5(b). For both cases, the modulation intensity along the time delay follows the periodicity of the half optical cycle of the IR laser ($T_{\rm IR}$). With the change of the CEP, the overall modulation structure undergoes a shift in time delay. We choose photon energies of 66.7 eV and 74.5 eV and extract data of the modulated HHG intensity as a function of the time delay. After fitting these data, obtained oscillating envelopes are plotted in Fig. 5(d). Vertical dotted lines are used to mark the position of the peak in each curve. For both photon energies, the extracted shift in the time delay due to the change of the CEP is 0.122 $T_{\rm IR}$, where $T_{\rm IR}$ is the period of the IR laser. Compared to electric fields of the 5-fs IR laser plotted in Fig. 5(c), the time shift is 0.125 $T_{\rm IR}$, which accounts for the change of the electric peak due to the change of the CEP. The reconstructed time delay or the CEP equivalently according to Eq. (8) has an error of 2.4%. Note that there is only one peak in the envelope of the time-delayed HHG modulation intensity in Fig. 5(d); we thus only obtain the relative change of the CEP, not the absolute one.

We next determine the absolute CEP of 0.5 π by taking advantage of special features in the HHG streaking spectra. Such simulated spectra are shown in Fig. 6(a). We choose two photon energies, and plot the envelope of the time-delayed modulation intensity in Fig. 6(b). One can clearly see two equivalent maximum peaks. This is the distinct feature at the

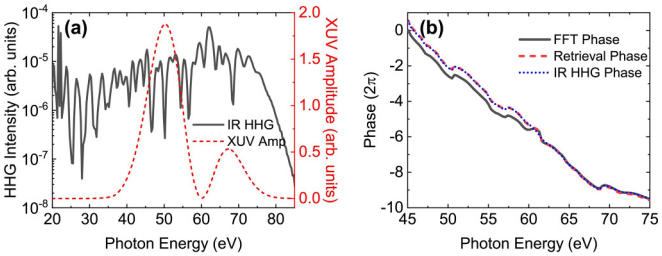

FIG. 7. (a) HHG spectrum (black solid line) by the IR laser alone and the spectral amplitude (red dashed line) of the shaped IAP. (b) The phase of modulated energy spectra (black solid line), and comparison of the retrieved HHG phase $\phi_1(\omega)$ by the IR laser alone and the numerically calculated one by the QRS model.

CEP of 0.5 π. Once two peaks are identified from experimental HHG streaking spectra, other absolute CEPs of the IR laser can be obtained by measuring the time shift of the maximum modulation intensity with respect to two peaks at the CEP of 0.5 π as demonstrated in Fig. 5.

IV. RECONSTRUCTION OF THE PHASE OF HIGH HARMONICS DRIVEN BY THE IR LASER ALONE

According to the EQRS model, the induced dipole moment $x(\omega, \tau)$ under the IAP and the time-delayed IR laser is mostly from two terms [22]. The first one is the induced dipole moment by the IR laser alone, which can be expressed as

$$x_1(\omega) = F(\omega)e^{i\phi_1(\omega)}. \tag{9}$$

Here, $F(\omega)$ is the spectral amplitude and $\phi_1(\omega)$ is the spectral phase of $x_1(\omega)$. The second one is the induced dipole moment due to coupling of the IAP and the IR laser, and can be written as

$$x_2(\omega, \tau) \propto \frac{\epsilon}{2} e^{i[\phi_{\rm XUV}(\omega)-\omega\tau]} E_{\rm IR}(\alpha - \tau), \tag{10}$$

where $\phi_{\rm XUV}(\omega)$ is the spectral phase of the IAP. We assume that the amplitudes of the two terms are comparable, and only keep the interference part. The intensity of HHG streaking spectra, i.e., $|x(\omega, \tau)|^2$, can be simplified as

$$S(\omega, \tau) \approx A^2 \cos[\phi_1(\omega) - \phi_{\rm XUV}(\omega) + \omega\tau]. \tag{11}$$

Equation (11) can be applicable for any CEPs of the few-cycle IR laser. We then perform the Fourier transform with respect to the time delay according to Eq. (1). The phase of modulated energy spectra is then written as [37]

$$\phi_{\rm mod}(\omega) = \phi_1(\omega) - \phi_{\rm XUV}(\omega). \tag{12}$$

Therefore, once the spectral phase of the IAP is correctly retrieved by the original (or improved) phase reconstruction method, the phase of HHG by the IR laser alone can also be retrieved from HHG streaking spectra.

We illustrate such an example in Fig. 7. Figure 7(a) shows HHG spectra (black solid line) driven by the single IR laser and the spectral amplitude distribution (red dashed line) of the shaped IAP. Here, phase information can only be obtained for high harmonics within the spectral region of the shaped IAP. Figure 7(b) shows the phase (black solid line) of modulated energy spectra, which is obtained by smoothly connecting the phase along the photon energy in Fig. 3(d). According to Eq. (12), by subtracting the phase of the shaped XUV pulse as shown in Fig. 3(b), the reconstructed phase $\phi_1(\omega)$ (red dashed line) can be obtained. It achieves a perfect agreement with the phase (blue dotted line) of single-IR HHG numerically calculated by the QRS model. Note that we can only reconstruct the phase of high harmonics by the IR laser alone, not the amplitude. Information on the amplitude can either be measured in an independent HHG experiment using the spectrometer or reconstructed from HHG streaking spectra by further improving the retrieval algorithm in the future.

V. SUMMARY

In summary, we modified the previously proposed all-optical phase reconstruction method by using HHG streaking spectra [22]. We were able to successfully retrieve the spectral phase of the shaped IAP, the CEP of the IR laser, and the phase of high harmonics by the IR laser alone. First, we used B-spline basis functions, employed the genetic algorithm, and defined the fitness function in terms of the phase of modulated energy spectra. It was combined with the previous phase reconstruction method to retrieve the spectral phase and "split" temporal information of shaped IAPs. Second, we included the CEP of the IR laser in the formulation for the reconstructed XUV phase; the CEP of 0.5 π can be identified from HHG streaking spectra first, and other absolute CEPs thus can be extracted. Third, we related the phase of modulated energy spectra to the spectral phase of the IAP and the phase of high harmonics by the IR laser alone. We showed that the phase of HHG by the single-IR laser can be precisely reconstructed if the spectral phase of the IAP is known (or accurately retrieved). This work greatly extends the applicability of the all-optical method based on the HHG streaking spectra.

ACKNOWLEDGMENTS

This work was supported by the National Natural Science Foundation of China (NSFC) under Grants No. 12274230 and No. 12204238, the Funding of Nanjing University of Science and Technology (NJUST) under Grant No. TSXK2022D005, and the Natural Science Foundation of Jiangsu Province under Grant No. BK20220925. C.D.L. was supported by the Chemical Science Division, Office of Basic Energy Sciences, Office of Science, US Department of Energy, under Grant No. DE-FG02-86ER13491.

[1] F. Krausz and M. Ivanov, Rev. Mod. Phys. **81**, 163 (2009).

[2] L. Y. Peng, W. C. Jiang, J. W. Geng, W. H. Xiong, and Q. H. Gong, Phys. Rep. **575**, 1 (2015).

[3] F. Calegari, G. Sansone, S. Stagira, C. Vozzi, and M. Nisoli, J. Phys. B **49**, 062001 (2016).

[4] H. Yun, S. J. Yun, G. H. Lee, and C. H. Nam, J. Phys. B **50**, 022001 (2017).

[5] P. M. Paul, E. S. Toma, P. Breger, G. Mullot, F. Augé, P. Balcou, H. G. Muller, and P. Agostini, Science **292**, 1689 (2001).
[6] M. Hentschel, R. Kienberger, C. Spielmann, G. A. Reider, N. Milosevic, T. Brabec, P. B. Corkum, U. Heinzmann, M. Drescher, and F. Krausz, Nature (London) **414**, 509 (2001).
[7] J. Li, X. M. Ren, Y. C. Yin, K. Zhao, A. Chew, Y. Cheng, E. Cunningham, Y. Wang, S. Y. Hu, Y. Wu, M. Chini, and Z. Chang, Nat. Commun. **8**, 186 (2017).
[8] T. Gaumnitz, A. Jain, Y. Pertot, M. Huppert, I. Jordan, F. Ardana-Lamas, and H. J. Wörner, Opt. Express **25**, 27506 (2017).
[9] V. S. Yakovlev, J. Gagnon, N. Karpowicz, and F. Krausz, Phys. Rev. Lett. **105**, 073001 (2010).
[10] Y. Mairesse and F. Quéré, Phys. Rev. A **71**, 011401(R) (2005).
[11] M. Chini, S. Gilbertson, S. D. Khan, and Z. H. Chang, Opt. Express **18**, 13006 (2010).
[12] X. Zhao, H. Wei, Y. Wu, and C. D. Lin, Phys. Rev. A **95**, 043407 (2017).
[13] X. Zhao, S. J. Wang, W. W. Yu, H. Wei, C. L. Wei, B. C. Wang, J. C. Chen, and C. D. Lin, Phys. Rev. Appl. **13**, 034043 (2020).
[14] K. Wang, B. C. Li, X. Y. Tang, C. H. Xu, C. D. Lin, and C. Jin, Phys. Rev. A **104**, 033102 (2021).
[15] A. C. Brown and H. W. van der Hart, Phys. Rev. Lett. **117**, 093201 (2016).
[16] M. Lewenstein, P. Balcou, M. Y. Ivanov, A. L'Huillier, and P. B. Corkum, Phys. Rev. A **49**, 2117 (1994).
[17] T. S. Sarantseva, M. V. Frolov, N. L. Manakov, A. A. Silaev, A. A. Romanov, N. V. Vvedenskii, and A. F. Starace, Phys. Rev. A **101**, 013402 (2020).
[18] G. T. Zhang, J. Wu, C. L. Xia, and X. S. Liu, Phys. Rev. A **80**, 055404 (2009).
[19] C. Serrat, Phys. Rev. Lett. **111**, 133902 (2013).
[20] C. Serrat, D. Roca, and J. Seres, Opt. Express **23**, 4867 (2015).
[21] C. Serrat, D. Roca, J. M. Budesca, J. Seres, E. Seres, B. Aurand, A. Hoffmann, S. Namba, T. Kuehl, and C. Spielmann, Opt. Express **24**, 8028 (2016).
[22] K. Wang, Y. Fu, B. C. Li, X. Y. Tang, B. C. Wang, Z. Guan, C. D. Lin, and C. Jin, New J. Phys. **25**, 083003 (2023).
[23] A. T. Le, R. R. Lucchese, S. Tonzani, T. Morishita, and C. D. Lin, Phys. Rev. A **80**, 013401 (2009).
[24] S. Minemoto, T. Umegaki, Y. Oguchi, T. Morishita, A. T. Le, S. Watanabe, and H. Sakai, Phys. Rev. A **78**, 061402(R) (2008).
[25] H. J. Wörner, H. Niikura, J. B. Bertrand, P. B. Corkum, and D. M. Villeneuve, Phys. Rev. Lett. **102**, 103901 (2009).
[26] J. P. Farrell, L. S. Spector, B. K. McFarland, P. H. Bucksbaum, M. Gühr, M. B. Gaarde, and K. J. Schafer, Phys. Rev. A **83**, 023420 (2011).
[27] J. Higuet, H. Ruf, N. Thiré, R. Cireasa, E. Constant, E. Cormier, D. Descamps, E. Mével, S. Petit, B. Pons, Y. Mairesse, and B. Fabre, Phys. Rev. A **83**, 053401 (2011).
[28] S. B. Schoun, R. Chirla, J. Wheeler, C. Roedig, P. Agostini, L. F. DiMauro, K. J. Schafer, and M. B. Gaarde, Phys. Rev. Lett. **112**, 153001 (2014).
[29] A. D. Shiner, B. E. Schmidt, C. Trallero-Herrero, P. B. Corkum, J. C. Kieffer, F. Légaré, and D. M. Villeneuve, J. Phys. B **45**, 074010 (2012).
[30] B. D. Bruner, Z. Masin, M. Negro, F. Morales, D. Brambila, M. Devetta, D. Facciala, A. G. Harvey, M. Ivanov, Y. Mairesse, S. Patchkovskii, V. Serbinenko, H. Soifer, S. Stagira, C. Vozzi, N. Dudovich, and O. Smirnova, Faraday Discuss. **194**, 369 (2016).
[31] N. Suárez, A. Chacón, J. A. Pérez-Hernández, J. Biegert, M. Lewenstein, and M. F. Ciappina, Phys. Rev. A **95**, 033415 (2017).
[32] M. Ruberti, P. Decleva, and V. Averbukh, Phys. Chem. Chem. Phys. **20**, 8311 (2018).
[33] C. Jin, S. J. Wang, X. Zhao, S. F. Zhao, and C. D. Lin, Phys. Rev. A **101**, 013429 (2020).
[34] C. Jin, S. J. Wang, S. F. Zhao, A. T. Le, and C. D. Lin, Phys. Rev. A **102**, 013108 (2020).
[35] C. Jin, G. L. Wang, A. T. Le, and C. D. Lin, Sci. Rep. **4**, 7067 (2014).
[36] C. Jin, X. X. Zhou, and S. F. Zhao, Commun. Theor. Phys. **44**, 1065 (2005).
[37] W. P. Dong, H. Y. Hu, and Z. X. Zhao, Opt. Express **28**, 22490 (2020).